INTL JOURNAL OF ELECTRONICS AND TELECOMMUNICATIONS, 2022, VOL. 70, NO. 4, PP. 839-847
Manuscript received August 19, 2024; revised October 2024. doi: 10.24425/ijet.2024.152068

Spectral Analysis of MRI Sound Signal

Swapnil Arawade, and Janusz Piechowicz

***Abstract*—Magnetic Resonance Imaging (MRI) is a very versatile diagnostic tool for non-invasive analysis of human organ functions, without use of ionizing radiations. Loud operating sound is the major challenge associated with the MRI technology, reaching up to 130dB. This paper analyses and compares the spectral properties of acoustic noise produced in the examination room of the mobile imaging trailer based 1.5 Tesla MRI system, during different scanning sequences of image acquisition. The analysis is useful in understanding the dynamic behavior of the sound generated inside the examination room to develop the noise reduction strategy.**

***Keywords*—magnetic resonance imaging; acoustics; spectral analysis**

I. Introduction

MAGNETIC Resonance (MR) Imaging (MRI) is a tool used to analyze the internal functions of human organs by utilizing a strong magnetic field and radio waves to produce detailed 3D images. MRI holds significant importance in the medical diagnosis field and is safer as it does not use harmful ionizing radiation [1]-[3]. One major challenge with MRI is the high acoustic noise levels associated with its operation. This noise is primarily caused by the generation of the Lorentz force (electromagnetic force) when electric current passes through the gradient coil in the presence of a strong static magnetic field. The clarity, spatial resolution, and quality of the acquired image are proportional to the magnetic field strength and the fast switching of the gradient field, leading to higher Lorentz forces and, consequently, higher acoustic noise levels. Studies have reported acoustic noise levels reaching above 130 dB during image acquisition in MRI systems with high magnetic field strength [4]-[11]. Along with psychological effects such as anxiety, stress, and hypertension, this noise can cause serious issues, including temporary or permanent hearing loss in patients [12]-[13]. The noise generated during MRI can also interfere with brain signal stimulation, potentially leading to incorrect results in functional MRI (fMRI) of the brain [14]-[16].

The use of hearing protection is mandatory for patients undergoing MRI scans. Although it reduces exposure to acoustic noise, it does not eliminate patient discomfort [17]-[18]. Noise reduction methods are divided into two categories: controlling the generation of sound and controlling the propagation of sound. Modifying and optimizing the electrical input to the gradient coil can reduce noise but often at the expense of image quality [19]. On the other hand, hardware modifications to control noise propagation can be financially expensive and technologically challenging [20]. Classical noise control strategies, such as enclosures, barriers, absorbers, and silencers, along with active noise cancellation systems, can provide more reliable solutions for reducing MRI noise [21]-[24].

The MRI system is surrounded by the air inside the examination room which acts as a medium for propagation of progressive sound waves generated during MRI. These waves are received by the human auditory system as a noise [25],[26]. This acoustic signal has harmonic characteristics and possess significant components of frequency spectrum in the audio frequency range. Due to the harmonic nature of the MRI acoustic signal, spectral analysis methods similar to those used for voiced speech signal analysis can be employed [27],[28].

The main motivation for this work was to compare the spectral properties of the acoustic noise generated near MRI equipment during image acquisition using different scanning sequences. The input parameters of the electrical signal provided to the gradient coil vary with different scanning sequences, leading to expected changes in the spectral properties of the acoustic noise. This study investigates the dynamic nature of the spectral properties between and within scanning sequences. The results will help tailor noise reduction strategies to make MRI more comfortable for patients and aid in designing acoustic walls to minimize the transfer of vibrations and acoustic noise to adjacent rooms, such as the control room [29]-[32].

II. Materials and Methods

A. Acoustic measurements (data collection):

The sound signal data was collected for 1.5 Tesla MRI system (Make: Phillips, Model: Ingenia 1.5 T MR) having maximum gradient strength of 45 mT/m and slew rate of 200.00 T/m/s at the test facility of JMP MEDICALS, Ostrów, Poland. The wave signal of noise generated during MRI was recorded with free field condenser omnidirectional microphone (SVANTEK 7052E) of ½ inch diameter with frequency range of 20-20000 Hz. The microphones were positioned at 2-meter distance from MRI isocenter at the height 30 cm above the patient bed and axis was aligned with MRI bed. The microphone was connected to the sound level meter (Make: SVANTEK, model: SVAN971) by shielded cable and controlled by Zoom H6. The doped water

This work was supported by the Faculty of Mechanical Engineering and Robotics, Department of Mechanics and Vibroacoustics, AGH University of Science and Technology, Al. Adama Mickiewicza 30, 30 - 059 Kraków, Poland from the finance source: 16.16.130.942.

S. Arawade and J. Piechowicz are with AGH University of Krakow. Faculty of Mechanical Engineering and Robotics, Department of Mechanics and Vibroacoustics, Poland (e-mail: sarawade@agh.edu.pl, ORCID: 0000-0003-1571-050X; piechowi@agh.edu.pl ,ORCID: 0000-0002-1435-4673).

phantom was kept in the MRI scanning cavity. The data collection setup is presented in the Fig. 1. The investigation was carried out for the scanning sequences, namely: Diffusion Weighted Imaging (DWI), Diffusion Weighted Imaging - Oscillating Gradient (DWI-OG), Diffusion Weighted Imaging - Turbo Spin Echo (DWI-TSE). The parameters of these sequences are listed in the Table 1.

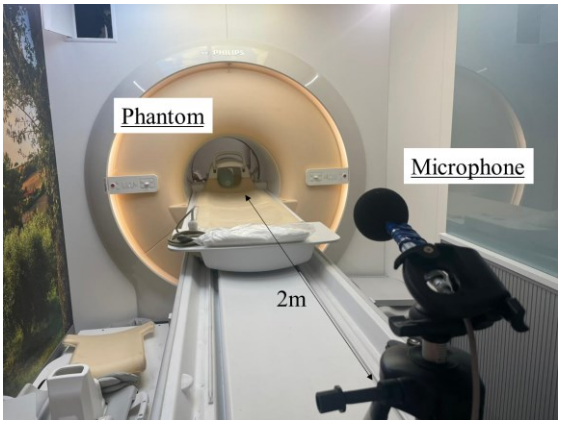

(a)

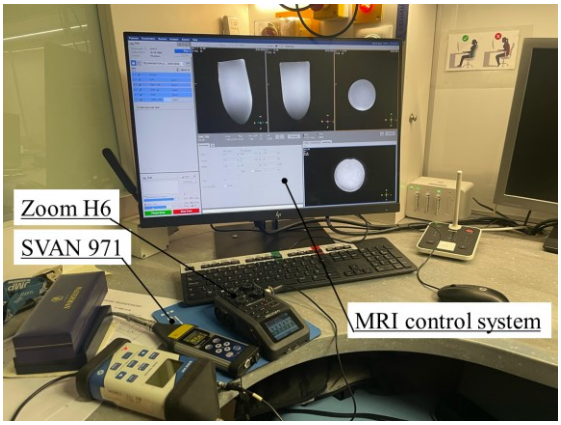

(b)

Fig.1. Sound measurement setup (a) Inside the examination room (b) Setup in control room

B. *Spectral analysis of the s MRI noise:*

A spectrogram is a best way to visualize the basic spectral properties in the signal processing. The interesting parts in the acoustic noise signal form MRI are identified as region of interest (ROIs) and are important for understanding the dynamic behavior of noise. In the preprocessing the recorded signals were normalized to amplitude to ensure the signals were in suitable format for the spectral analysis. The normalized amplitude of signal is denoted by $s(t)$. The smoothed spectra of the signal can be calculated by using the Welch's method. The periodogram of the signal indicating the estimate of the power spectral density (PSD) is calculated from N_{FFT} −point Fast Fourier Transform (FFT), where N_{FFT} represents the number of points for Fourier transform evaluation. The obtained PSD from N_{FFT} −point FFT is expressed in the logarithmic scale as dB/Hz .The difference between the PSDs of the signals can be estimated by spectral distance (D_{RMS}) evaluated in dB as the root mean squared value up to one half of the sampling frequency (f_s). The mathematical formulation for the PSD estimation using the Welch's method is shown in Eq. (1).

$$P_{xx}(f) = \frac{1}{L}\sum_{i=0}^{K-1}\left(\mathrm{F}\left(w(n)x_i(n)\right)\right)^2 \quad (1)$$

where $P_{xx}(f)$ is the power spectral density which is function of frequency (f) , F denotes the Fourier transform, $w(n)$ is the window function, $x_i(n)$ is the i^{th} segment of the signal, K is the number of segments and L is the length of each segment.

In addition to the basic spectral properties such as spectral centroid and spread, the complimentary spectral properties such as spectral skewness, kurtosis, and spectral flatness. These properties provide deeper insights about the characteristics of the sound signal.

The expression for the spectral centroid (C) is calculated as follows:

$$C = \frac{\sum_{i=0}^{N-1} f_i P_{xx}(f_i)}{\sum_{i=0}^{N-1} P_{xx}(f_i)} \quad (2)$$

where, N is number of frequency bins in the signal.

The spectral spread (σ) is calculated using the following equation:

$$\sigma = \sqrt{\frac{\sum_{i=0}^{N-1} (f_i - C)^2 P_{xx}(f_i)}{\sum_{i=0}^{N-1} P_{xx}(f_i)}} \quad (3)$$

The expression for Spectral skewness (SS) is presented as follows:

$$SS = \frac{\sum_{i=0}^{N-1} \left(\frac{f_i - C}{\sigma}\right)^3 P_{xx}(f_i)}{\sum_{i=0}^{N-1} P_{xx}(f_i)} \quad (4)$$

TABLE I
SUMMARY OF THE SCANNING SEQUENCES USED IN 1.5 TESLA MRI SCANNER

Sr. No	Quantity	DWI	DWI-TSE	DWI-OG	Unit
1	Static field strength, (B0)	1.5	1.5	1.5	Tesla (T)
2	Repetition time, (TR)	2623	3329	2957	milliseconds
3	Echo time, (TE)	83	72	85	milliseconds
4	Number of slices	22	18	22	-
5	Slice thickness	1	1	1	millimeters (mm)
6	Field-of-view	79x79 x131	230x196 x107	230x230 x131	millimeters (mm)
7	Duration (T)	36	261	36	Seconds (sec)

Table shows the configuration of the 1.5 MRI scanner sequences

The expression for Spectral kurtosis (SK) is calculated using

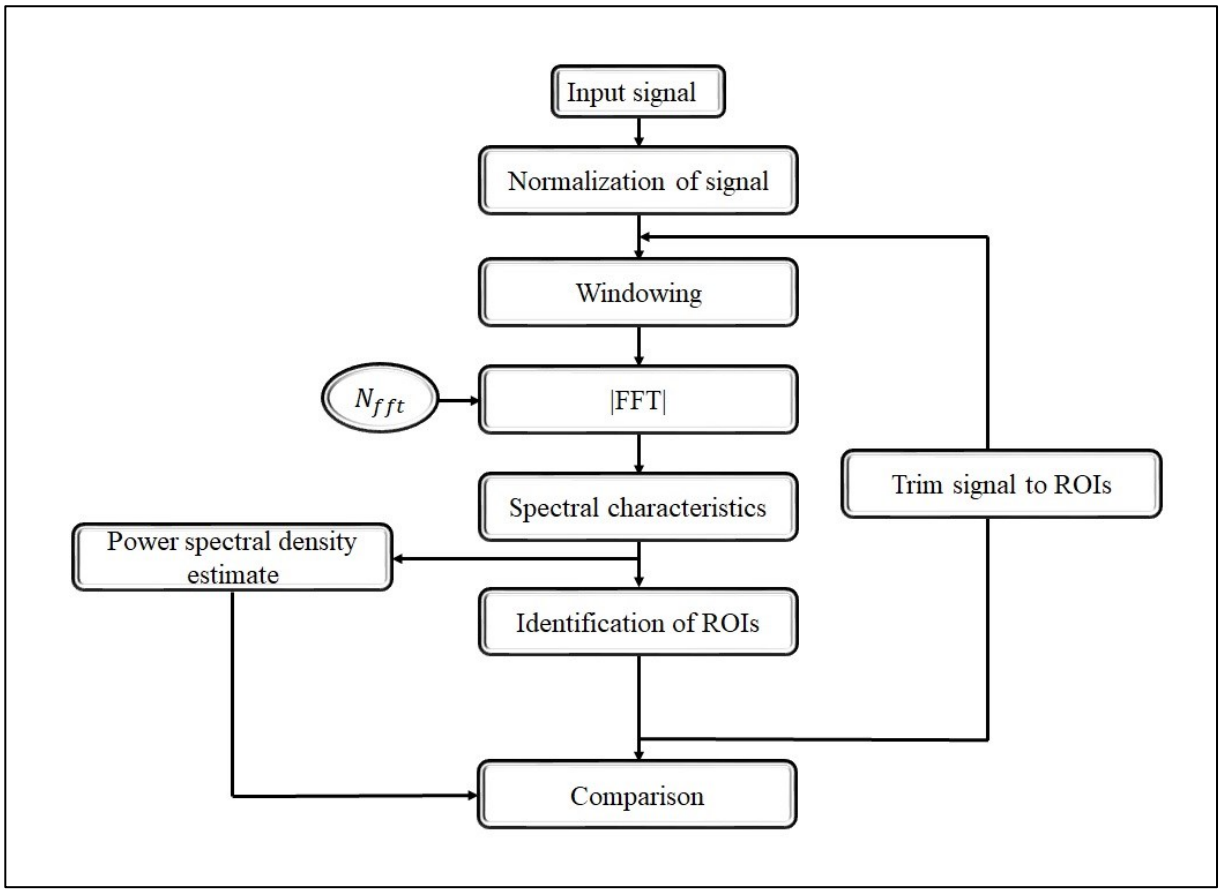

Fig. 2. Flow chart of spectral analysis

the following relation:

$$SK = \frac{\sum_{i=0}^{N-1}\left(\frac{f_i - C}{\sigma}\right)^4 P_{xx}(f_i)}{\sum_{i=0}^{N-1} P_{xx}(f_i)} \quad (5)$$

Spectral Flatness (SF) is calculated using the following equation:

$$SF = \frac{\exp\left(\frac{1}{N}\sum_{i=0}^{N-1} \ln P_{xx}(f_i)\right)}{\frac{1}{N}\sum_{i=0}^{N-1} P_{xx}(f_i)} \quad (6)$$

The spectral skewness evaluates the asymmetry of the power distribution around the spectral centroid indicating presence of outliners in the frequency domain. Spectral kurtosis measures the multi-peaks of the spectral revealing the extremity of deviation from normal distribution. Spectral flatness is the measure of the periodicity of the sound signal comparing the geometric mean to the arithmetic mean of the PSD. The flowchart of the analysis is presented in the Fig. 2.

III. Results

The acoustic noise generated by the MRI scanner in the examination room, during the different scanning sequences such as DWI, DWI-OG, DWI-TSE were recorded. The sampling frequency the measurement system was set to be 12000 Hz. The WAVE data of the sound signals were stored and transferred to computer from the sound level meter. Before analysis the sound signal were preprocessed. The preprocessing of the signal involved normalization of the signal which was important aspect to ensure uniformity of the signals for comparison of the spectral properties. The normalized amplitude of the signal is represented by $s(t)$ over the duration of recording and the waveforms of the recorded sound signal using the microphones during the different scanning sequences are shown in figure 3. As shown in Fig. 3, the spectrograms of the signal were evaluated to depict the dynamics of the frequency content of the signals for all scanning sequences. The power intensity in the spectrogram is represented as dB relative to 1 Pa^2 / Hz.

The single sided FFT spectrum referring to the half of the sampling frequency was evaluated for the waveforms of all sequences and are shown in the figure 4. The Welch's method was incorporated to obtain the smoothened spectral envelope of the signal to identify the dominant frequencies with high power spectral density. The frame duration of for computation of PSD was taken to be 25 milliseconds and the hamming window was applied to each segment under analysis. The overlap coefficient of the frames was taken to be 75 % in order to improve the frequency resolution of the PSD. The comparison of the Welch's power spectral density estimate calculated for the DWI, DWI-OG and DWI-TSE is shown in the Fig. 5. The statistical comparison of the spectral flatness evaluated for different scanning sequences is depicted in the Fig. 6.

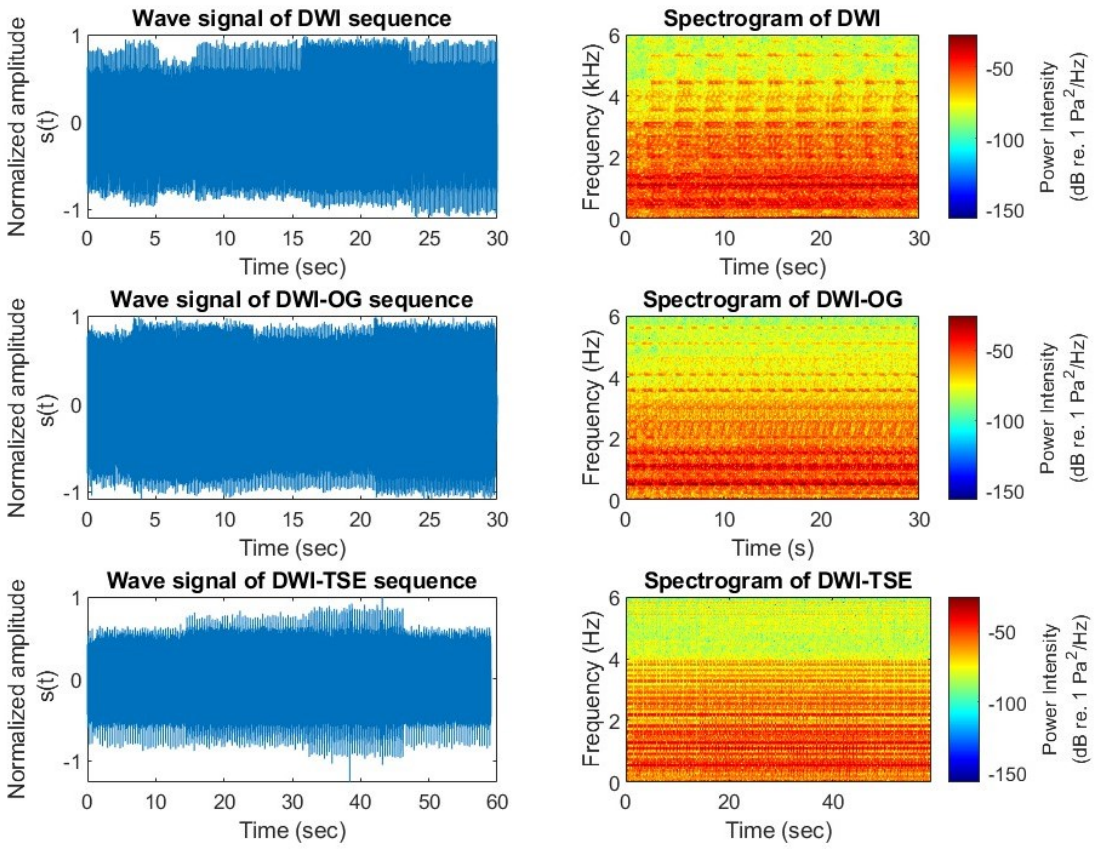

Fig. 3. Normalized waveform of acoustic signals and their respective spectrograms

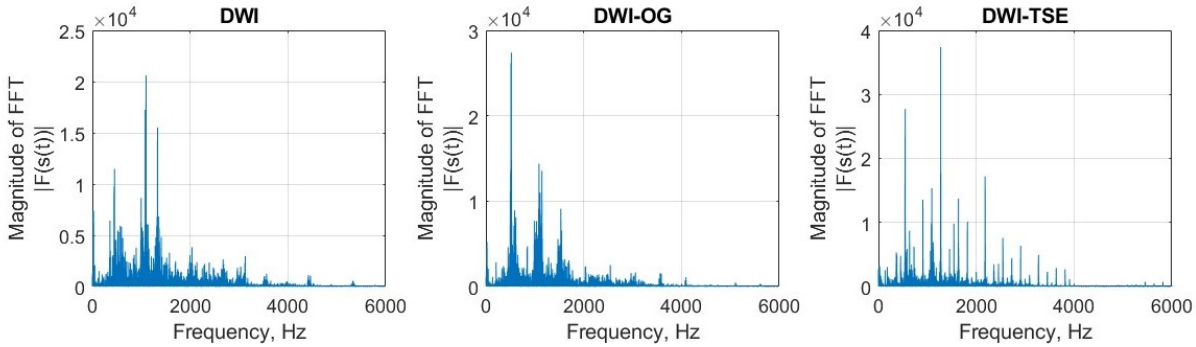

Fig. 4. Single sided FFT spectrum of the acoustic noise during DWI, DWI-OG, and DWI-TSE sequence

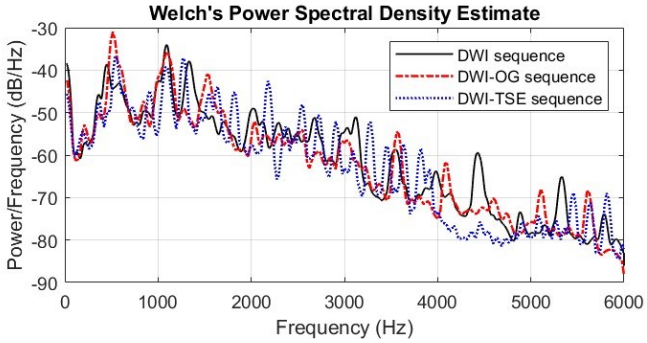

Fig. 5. Comparison of PSD estimate by Welch's method

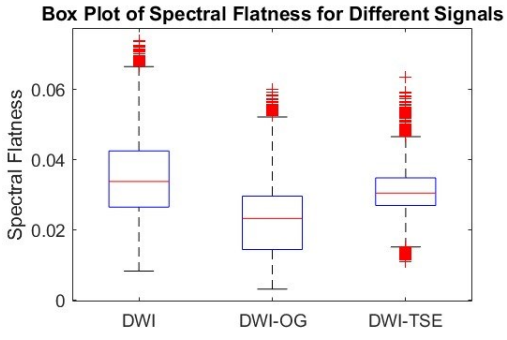

Fig. 6. Comparison of spectral flatness of signals

TABLE II
RESULTS FROM SPECTRAL ANALYSIS OF COMPLETE ACOUSTIC NOISE SIGNAL FOR DWI, DWI-OG, AND DWI-TSE

Scanning sequence	Dominant frequencies (Hz)			Spectral features			
	(1)	(2)	(3)	Spectral centroid	Spectral spread	Spectral skewness	Spectral Kurtosis
DWI	1091.9	1333.4	450.42	1055.1983 (Hz)	592.014 (Hz)	1.4468	8.3546
DWI-OG	512.63	1101.6	1523.4	834.058 (Hz)	482.9576 (Hz)	2.1214	11.7917
DWI-TSE	539.06	1265.6	1078.1	1162.3818 (Hz)	653.644 (Hz)	1.1726	5.348

The spectral analysis revealed the distinct characteristics for DWI, DWI-OG, and DWI-TSE scanning sequence. Each sequence shows unique dominant frequencies and spectral features as represented in the Table 2. It was observed that the dominant frequencies are varying in between 450 Hz to 1525 Hz. Notable, DWI-OG had highest spectral skewness (2.1214) and kurtosis (11.7917), indicating a more asymmetrical and peaked spectral distribution compared to others.

The spectral analysis of the region of interest with shorter duration allows to detect the transient events which might be averaged out of missed in a longer signal analysis. This is particularly important in developing the noise reduction strategy. The 2 second duration ROIs in the acoustic noise signal were identified visually and considered for spectral analysis as shown in the Fig. 7, which depicts identification of ROIs in the acoustic signal from DWI sequence.

The comparison of the ROIs in each sequences DWI, DW-OG, and DWI-TSE is presented in the Fig. 8. The difference between the PSD of the ROIs was calculated with spectral distance. The D_{RMS} for the ROI_1 and ROI_2 are 3.91 dB, 2.34 dB and 6.91 dB for scanning sequence DWI, DWI-OG, and DWI-TSE respectively. The spectral flatness of the ROIs was compared and presented in the figure 8, which depicts variation in the flatness measure withing the signal. All the spectral flatness measures for the ROIs of sequences are less than 0.1 indicating the voiced nature of the signal. The spectral properties such as spectral centroid, spectral spread, spectral skewness, and spectral kurtosis are listed in the Table 3. The ROIs of DWI-OG were observed to have high spectral kurtosis as compared to other, indicating the strong noise during the sequence.

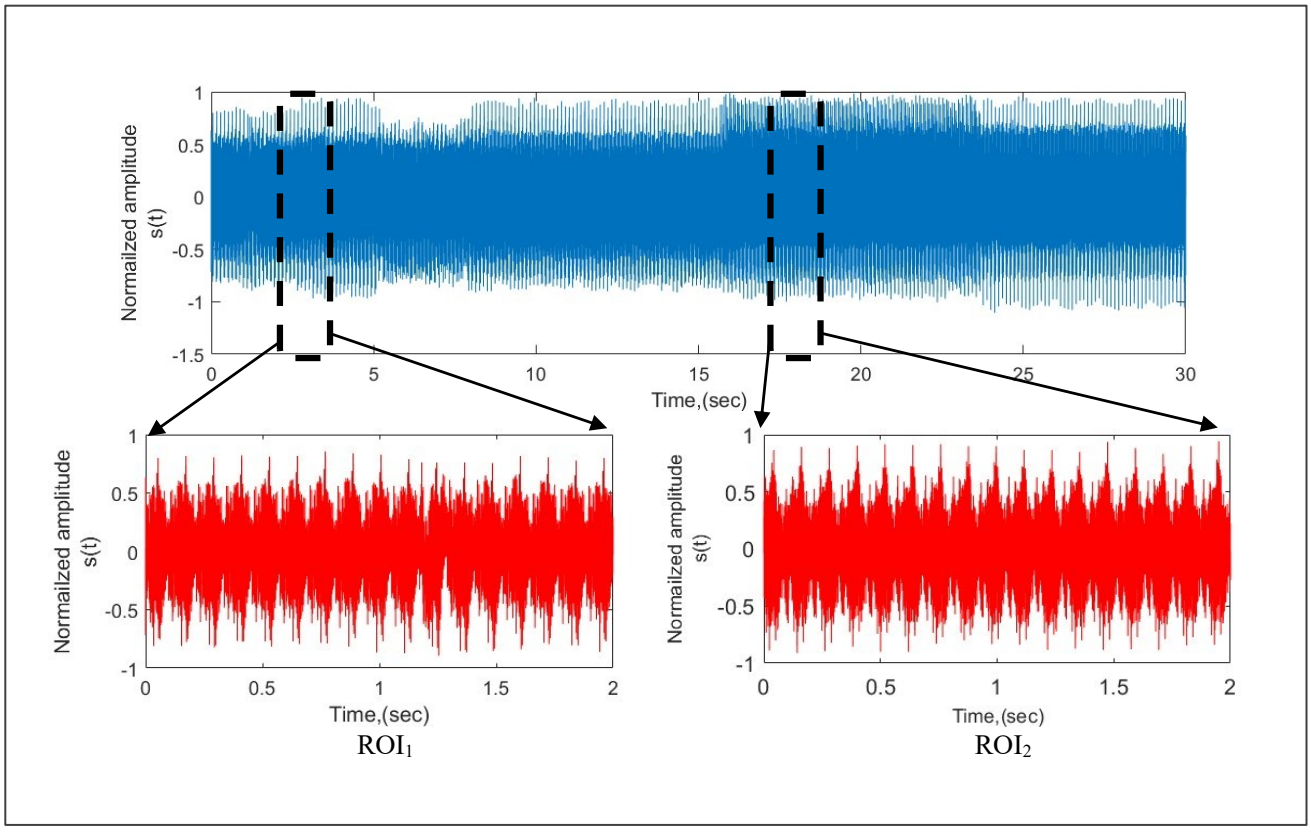

Fig. 7. Depiction for identification of ROI in the DWI sequence

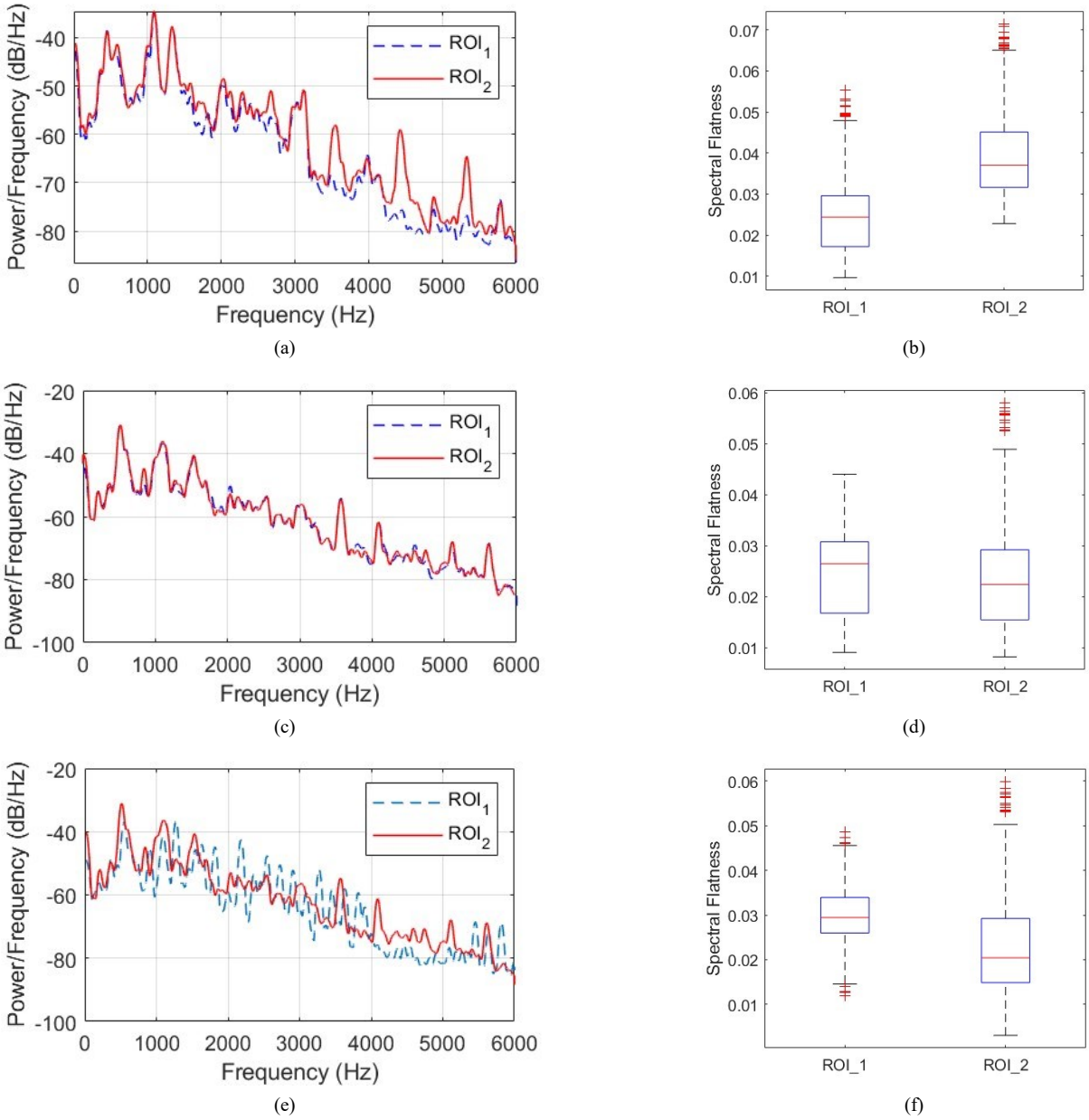

Figure 8. Comparison of ROIs of acoustic noise, (a) PSD comparison of ROIs in DWI sequence, (b) Spectral flatness of the ROIs in DWI, (c) PSD comparison of ROIs in DWI-OG sequence, (d) Spectral flatness of the ROIs in DWI-OG, (e) PSD comparison of ROIs in DWI-TSE sequence, and (f) Spectral flatness of the ROIs in DWI-TSE.

TABLE III
COMPARISON OF SPECTRAL PROPERTIES OF THE ROIS OF ACOUSTIC NOISE DURING DWI, DWI-OG, AND DWI-TSE

Sequence	Region of Interest (ROI)	Spectral Centroid (Hz)	Spectral Spread (Hz)	Spectral Skewness	Spectral Kurtosis
DWI	ROI 1	1075.5646	536.8498	1.3755	7.7733
	ROI 2	1082.1688	593.4671	1.584	8.52
DWI-OG	ROI 1	828.1218	488.7577	2.2762	11.9522
	ROI 2	843.5903	489.9879	1.9617	11.081
DWI-TSE	ROI 1	1200.0907	666.1893	1.1178	4.9512
	ROI 2	830.1233	483.9986	2.0782	11.6263

IV. Discussion

The comprehensive spectral analysis of MRI sound signals performed for three different scanning sequences (DWI, DWI-OG, and DWI-TSE) offers deep insights into their spectral characteristics. These findings have revealed significant implications for diagnostic imaging as well as therapeutic applications, specifically in the development of noise reduction strategies in the MRI scanning room, which can enhance patient comfort and the overall MRI experience as well as ensuring safety of the staff in adjacent room by reduction of transmission of the noise.

The spectral centroid values from the three scanning sequences under analysis show distinct difference in their frequency content, revealing the critical insights into the energy distribution of the signals. Here, DWI and DWI-TSE have higher spectral centroids (1055.1983 Hz and 1162.3818 Hz, respectively) compared to DWI-OG (834.058 Hz). This implies that DWI and DWI-TSE scans possess higher frequency components, likely due to the specific gradient encoding and the rapid switching of gradients inherent in these sequences. The low value of the centroid in DWI-OG indicates the dominance of lower frequency components, which is likely resulting from the absence of rapid gradient switching. DWI and DWI-TSE contribute to the perceived loudness and discomfort during the MRI scans because of their higher frequency components. Analysis of the spectral spread revealed the dispersion of the spectrum around its centroid, which provided a measure of the frequency bandwidth of the signal. DWI-TSE exhibits the highest spectral spread (653.644 Hz), followed by DWI (592.014 Hz) and DWI-OG (482.9576 Hz). The broader spread in DWI-TSE implies effect of the additional gradient and radio-frequency pulses used in turbo spin echo sequences, which is main cause for a wider range of frequencies. The narrower spread in DWI-OG suggests a highly concentrated frequency distribution, arising due to its simpler gradient structure. The broader spectral spread in DWI-TSE reveals the complex acoustic environment, which poses a challenge for noise reduction but also provides an opportunity to design more effective noise absorption panels tailored to these specific frequency ranges [33]-[35].

Results from the analysis of spectral skewness and kurtosis provided insights into the shape and symmetry of the spectral distribution. DWI-OG presented the highest spectral skewness (2.1214) and kurtosis (11.7919), resulting a more asymmetric and peaked spectrum. This implies the predominance of frequency components in DWI-OG, resulting from gradient interactions that emphasize specific frequencies. In contrast, DWI and DWI-TSE have lower skewness and kurtosis values, suggesting more symmetrical and flatter spectral distributions. Spectral flatness depicted the uniformity of the power spectrum during the scanning sequences. The analysis indicates varying degrees of flatness among the sequences, with DWI-OG having a lower spectral flatness, which indicates a peakier spectrum. This confirms with its higher skewness and kurtosis. DWI and DWI-TSE, with higher spectral flatness, exhibit more uniform spectral characteristics, indicating a more balanced distribution of power across frequencies. For all scanning sequences the overall spectral flatness we observed to be lower than 0.1, which signifies that the sound signal is tonal, with very pronounced peak in its frequency spectrum. This implies that the most of signal's energy is concentrated about certain specific frequencies making it less noise like and more alike the pure tones. The low spectral flatness reveals that the noise has distinct tonal components, which could be more discomforting to the patient under examination as compared to more uniform noise distribution. These findings are crucial for understanding the asymmetry and peakiness of the spectral distribution, which can guide the selection of materials and structures that are most effective in absorbing these specific frequencies [36],[37].

Further analysis of specific ROIs within the sound signals provides deeper insights into localized spectral characteristics. The ROI analysis highlights the importance of evaluation of the localized spectral features, as they reveal subtle differences in signal behaviour that may not be apparent in the overall spectral analysis. The RMS spectral distance between the ROIs showed notable difference, emphasizing the distinct spectral properties associated with each scanning sequence. The values of D_{RMS} indicates the DWI-OG sequence is most spectrally similar among the three sequences, which indicates consistent spectral profile within the sequence. While, DWI-TSE has highest D_{RMS} of 6.91 dB indicating most variation in spectral characteristics of ROIs. The spectral properties of the ROIs in the DWI and DWI-TSE sequence have higher spectral centroids and spread, revealing that these regions are brighter and gave more varied frequency content. ROIs in the DWI-OG sequence are characterised by higher skewness and kurtosis highlighting their asymmetrical and peaked spectral nature. This localised analysis reveals the dynamic nature of the signals and are crucial for identification of specific frequency bands that require targeted absorption. By focusing on these critical areas, the effectiveness of noise reduction can be significantly enhanced, leading to a quieter and more comfortable MRI environment.

V. Conclusion

This study presents a detailed spectral analysis of MRI sound signals generated by a 1.5 Tesla MRI scanner recorded from three distinct scanning sequences: DWI, DWI-OG, and DWI-TSE. A comprehensive analysis of the basic and complementary spectral characteristics was performed. The power spectral density of the signal was evaluated using Welch's method, and the dominant frequencies associated with the scanning sequences were identified to vary between 450 Hz and 1525 Hz. The DWI-OG sequence revealed the highest spectral skewness (2.1214) and kurtosis (11.7917), indicating a more asymmetrical and peaked spectral distribution compared to others. To obtain a more detailed analysis of the signals, the ROIs of 2 seconds were identified, and spectral characteristics were evaluated and compared within the same scanning sequences. The analysis of ROIs revealed a high spectral distance in the DWI-TSE sequence, indicating a significant difference in spectral profile, while DWI-OG ROIs showed a consistent spectral profile. The spectral flatness (Weiner entropy) analysis revealed that DWI and DWI-TSE sequences possess higher flatness, indicative of a more uniform frequency distribution, whereas DWI-OG's lower flatness denotes a more pronounced peak. The overall spectral flatness for all sequences was identified to be below 0.1, indicating the signal's energy is concentrated around specific frequencies. The focused analysis of ROIs within the sound signals allowed for a granular understanding of localized spectral features. This is particularly

valuable for designing noise absorption panels tailored to specific frequency bands, enhancing noise reduction, and improving patient comfort during MRI. Future work should explore advanced materials and methods to further optimize acoustic environments in MRI facilities, ensuring both operational efficiency and patient comfort.

ACKNOWLEDGEMENTS

This work was supported and financed by Department of Mechanics and Vibroacoustics, Faculty of Mechanical Engineering and Robotics, AGH University of Science and Technology in Kraków, Poland, from the finance source: 16.16.130.942. We also show gratitude towards Szymon Łoś, from the JMP Medicals, Ostrow Wielkopolski for support in measurement and experimentation.

REFERENCES

[1] F. Bruno, F. Arrigoni, S. Mariani, et al., "Advanced magnetic resonance imaging (MRI) of soft tissue tumors: techniques and applications," Radiol med 124, 243–252, 2019. https://doi.org/10.1007/s11547-019-01035-7

[2] R. Reda, A. Zanza, A. Mazzoni, A. Cicconetti, L. Testarelli, D. Di Nardo, "An update of the possible applications of magnetic resonance imaging (MRI) in dentistry: a literature review," Journal of imaging, vol-7(5), pp. 75. Apr. 2021. https://doi.org/10.3390/jimaging7050075

[3] L. Landini, L. T. Mainardi, V. Positano, A. A. Young, M. Santarelli, L. Ying, W. E. Kyriakos, A. J. den Dekker, M. Styner, Y. O. Halchenko, A. Frangi, "Advanced image processing in magnetic resonance imaging," CRC press, Oct. 3, 2018. https://doi.org/10.1201/9781420028669

[4] M. J. Nyrhinen, V. H. Souza, R. J. Ilmoniemi, F. H. Lin, "Acoustic noise generated by TMS in typical environment and inside an MRI scanner," Brain Stimulation, 17(2), pp. 184-193, Feb. 9, 2024. https://doi.org/10.1016/j.brs.2024.02.006

[5] L. Shtrepi, V. Poggetto, C. Durochat, M. Dubois, D. Bendahan, F. Nistri, M. Miniaci, N. M. Pugno, F. Bosia, "Acoustic noise levels and field distribution in 7 T MRI scanners," Frontiers in Physics,11, 14 Nov. 2023. https://doi.org/10.3389/fphy.2023.1284659

[6] P. Mansfield, P.M. Glover, J. Beaumont, "Sound generation in gradient coil structures for MRI," Magn Reson Med, vol. 39, issue 4, pp. 539–550, Apr. 1998. https://doi.org/10.1002/mrm.1910390406

[7] J.M. Jackson, "Pro-active acoustic noise reduction for magnetic resonance imaging scanners," PhD thesis, University of Tasmania, 2012. https://doi.org/10.25959/23204969.v1

[8] J.R. Foster, D.A. Hall, A.Q. Summerfield, A.R. Palmer, R.W. Bowtell, "Sound-level measurements and calculations of safe noise dosage during EPI at 3 T," J Magn Reson Imaging, 12(1), pp. 157-163. https://doi.org/10.1002/1522-2586(200007)12:1<157::AID-JMRI17>3.0.CO;2-M

[9] A. Moelker, P.M.T. Pattynama, "Acoustic noise concerns in functional magnetic resonance imaging," Hum. Brain Mapping, 20(3), pp. 123-141, 2003. https://doi.org/10.1002/hbm.10134

[10] J. Hutter, A.N. Price, L. Cordero-Grande, "Quiet echo planar imaging for functional and diffusion MRI," Magn ResonMed, 79(3), pp. 1447-1459, 2018. https://doi.org/10.1002/mrm.26810

[11] R.A. Hedeen, W.A. Edelstein, "Characterization and prediction of gradient acoustic noise in MR imagers," Magn Reson Med, 37, pp. 7–10, 1997. https://doi.org/10.1002/mrm.1910370103

[12] S.A. Counter, A. Olofsson, H.F. Grahn, & E. Borg, "MRI acoustic noise: sound pressure and frequency analysis," J Magn Reson Imaging, 7(3), pp. 606-611, 1997. https://doi.org/10.1002/jmri.1880070327

[13] R.E. Brummett, J.M. Talbot, P. Charuhas, "Potential hearing loss resulting from MR imaging," Radiology, 169(2), pp. 539- 540, Nov. 1988. https://doi.org/10.1148/radiology.169.2.3175004

[14] G. Pellegrino, A.L. Schuler, G. Arcara, G. Di Pino, F. Piccione & E. Kobayashi, "Resting state network connectivity is attenuated by fMRI acoustic noise," Neuroimage, 247, pp. 118791, Feb. 2022. https://doi.org/10.1016/j.neuroimage.2021.118791

[15] D. Tomasi, E.C. Caparelli, L. Chang & T. Ernst, "fMRI-acoustic noise alters brain activation during working memory tasks," Neuroimage, 27(2), pp. 377-38, 2005. https://doi.org/10.1016/j.neuroimage.2005.04.010

[16] T. Wolak. K. Cieśla, M. Rusiniak, A. Piłka, M. Lewandowska, A. Pluta, H Skarżyński, P.H. Skarżyński, "Influence of acoustic overstimulation on the central auditory system: An functional magnetic resonance imaging (fmri) study," Medical Science Monitor: International Medical Journal of Experimental and Clinical Research, 22, pp. 4623, 2016. https://doi.org/10.12659%2FMSM.897929

[17] M.J. McJury, "Acoustic Noise and Magnetic Resonance Imaging: A Narrative/Descriptive Review," J Magn Reson Imaging, 55, pp. 337-346, Feb. 2022. https://doi.org/10.1002/jmri.27525

[18] E. Kanal, F.G. Shellock, "Policies, guidelines, and recommendations for MR imaging safety and patient management," J Magn Reson Imaging, 2, pp.247–248, 1992. https://doi.org/10.1002/jmri.1880020222

[19] Y. Wang, P. Xu, J. Zeng, J. Zhang, Y. Zhu, S. Che, C. Yao, Y. Ge, C. Wang, "Sequence optimization for MRI acoustic noise reduction," In Journal of Physics: Conference Series, IOP Publishing, vol. 2591, no. 1, pp. 012034, Sept. 2023. DOI 10.1088/1742-6596/2591/1/012034

[20] F. Hennel, "Fast spin echo and fast gradient echo MRI with low acoustic noise," J Magn Reson Imaging,13(6), pp. 960–966, 2001. https://doi.org/10.1002/jmri.1138

[21] M.H. AlMeer, "MRI Acoustic Noise cancellation using CNN," Journal of Engineering Research, 2022. https://doi.org/10.36909/jer.17661

[22] M. Li, B. Rudd, T.C. Lim, J.H. Lee, "In situ active control of noise in a 4T MRI scanner," J Magn Reson Imaging, 34, pp. 662-669, Jul. 2011. https://doi.org/10.1002/jmri.22694

[23] N. Lee, Y. Park & G.W. Lee, "Frequency-domain active noise control for magnetic resonance imaging acoustic noise," Applied Acoustics, 118, pp. 30-38, 2017. https://doi.org/10.1016/j.apacoust.2016.11.003

[24] A. Lasota & M. Meller, "Iterative learning approach to active noise control of highly autocorrelated signals with applications to machinery noise," IET Signal Processing, 14(8), pp. 560-568, 2020. https://doi.org/10.1049/iet-spr.2020.0064

[25] G. Z. Yao, C. K. Mechefske, B. K. Rutt, "Acoustic noise simulation and measurement of a gradient insert in a 4 T MRI," Applied Acoustics, 66(8), pp. 957-73, Aug. 2005. https://doi.org/10.1016/j.apacoust.2004.11.006

[26] T. Hamaguchi, T. Miyati, N. Ohno, T. Matsushita, T. Takata, Y. Matsuura, S. Kobayashi, T. Gabata, "Spatial analysis of acoustic noise transfer function with a human-body phantom in a clinical MRI scanner," Acta Radiologica, 64(3), pp. 1212-1221, Mar. 2023. https://doi.org/10.1177/02841851221100079

[27] J. Wang, H. Liu, C. Zheng & X. Li, "Spectral subtraction based on two-stage spectral estimation and modified cepstrum thresholding," Applied acoustics, vol. 74, issue. 3, pp. 450-458, 2013. https://doi.org/10.1016/j.apacoust.2012.09.004

[28] J. Přibil, A. Přibilová, & I. Frollo, "Vibration and noise in magnetic resonance imaging of the vocal tract: Differences between whole-body and open-air devices," Sensors, 18(4), pp. 1112, Apr. 2018. https://doi.org/10.3390/s18041112

[29] H. Guo, W. Chen, Y. Wang, F. Ma, P. Sun, T. Yuan, T, & X. Xie, "Parametric modeling and deep learning-based forward and inverse design for acoustic metamaterial plates," Mechanics of Advanced Materials and Structures, pp. 1-11, Mar. 2024. https://doi.org/10.1080/15376494.2024.2330488

[30] B. Assouar; M. Oudich; X. Zhou, "Acoustic metamaterials for sound mitigation," Comptes Rendus. Physique, vol. 17, no. 5, pp. 524-532, 2017. https://doi.org/10.1016/j.crhy.2016.02.002

[31] M. Ghassabi, F. Motaharifar, R. Talebitooti, "Improving soundproof characteristics of an FG-CNT–reinforced composite structure by adding a coating magneto-electro-elastic layer," Journal of Vibration and Control, vol.30(7-8), pp. 1802-1817, Apr. 27 2024. https://doi.org/10.1177/10775463231171671

[32] M. Ghafouri, M. Ghassabi, M. R. Zarastvand, & R. Talebitooti, "Sound propagation of three-dimensional sandwich panels: influence of three-dimensional Re-entrant auxetic core," AIAA Journal, vol. 60, no. 11, pp. 6374–6384, Nov. 2022. https://doi.org/10.2514/1.J061219

[33] Y. S. Tsay, J. Y. Lin, F. Ma, "Development of a panel membrane resonant absorber," Applied Sciences, vol.11, no. 4, pp. 1893, Feb. 21 2021. https://doi.org/10.3390/app11041893

[34] X. Shao, X. Yan, “Sound absorption properties of nanofiber membrane-based multi-layer composites,” Applied Acoustics, 200, pp. 109029, Nov. 2022. https://doi.org/10.1016/j.apacoust.2022.109029

[35] I. Davis, A. McKay, G. J. Bennett, “A graph-theory approach to optimisation of an acoustic absorber targeting a specific noise spectrum that approaches the causal optimum minimum depth,” Journal of Sound and Vibration, vol. 505, pp.116135, Aug. 2021. https://doi.org/10.1016/j.jsv.2021.116135

[36] K. Meena, K. Soni, G. Moona, M. Singh, “Investigations on Sound Absorption Properties of Perforated Designed Panels for the Selective Frequency Absorption,” in International Conference On" Advances In Metrology", Singapore: Springer Nature Singapore, pp. 85-94, Aug 2022. https://doi.org/10.1007/978-981-99-4594-8_9

[37] C. Yu, X. Chen, M. Duan, M. Li, X. Wang, Y. Mao, L. Zhao, F. Xin, T. J. Lu, “Adjustable sound absorbing metastructures for low-frequency variable discrete sources,” International Journal of Mechanical Sciences. vol. 267, pp. 108965, Apr. 2024. https://doi.org/10.1016/j.ijmecsci.2024.108965